Neuron
Article

A Unique Population of Ventral Tegmental Area Neurons Inhibits the Lateral Habenula to Promote Reward

Alice M. Stamatakis,[1,2,3] Joshua H. Jennings,[1,2,3] Randall L. Ung,[2] Grace A. Blair,[2] Richard J. Weinberg,[3,4] Rachael L. Neve,[5] Frederick Boyce,[6] Joanna Mattis,[7] Charu Ramakrishnan,[7] Karl Deisseroth,[7] and Garret D. Stuber[1,2,3,4,8,*]
[1]Neurobiology Curriculum
[2]Department of Psychiatry
[3]Neuroscience Center
[4]Department of Cell Biology and Physiology
University of North Carolina at Chapel Hill, Chapel Hill, NC 27599, USA
[5]Department of Brain and Cognitive Science, Massachusetts Institute of Technology, Cambridge, MA 02139, USA
[6]Department of Neurology, Massachusetts General Hospital, Boston, MA 02114, USA
[7]Department of Bioengineering, Stanford University, Stanford, CA 94305, USA
[8]Bowles Center for Alcohol Studies, University of North Carolina at Chapel Hill, Chapel Hill, NC 27599, USA
*Correspondence: gstuber@med.unc.edu
http://dx.doi.org/10.1016/j.neuron.2013.08.023

SUMMARY

Lateral habenula (LHb) neurons convey aversive and negative reward conditions through potent indirect inhibition of ventral tegmental area (VTA) dopaminergic neurons. Although VTA dopaminergic neurons reciprocally project to the LHb, the electrophysiological properties and the behavioral consequences associated with selective manipulations of this circuit are unknown. Here, we identify an inhibitory input to the LHb arising from a unique population of VTA neurons expressing dopaminergic markers. Optogenetic activation of this circuit resulted in no detectable dopamine release in LHb brain slices. Instead, stimulation produced GABA-mediated inhibitory synaptic transmission, which suppressed the firing of postsynaptic LHb neurons in brain slices and increased the spontaneous firing rate of VTA dopaminergic neurons in vivo. Furthermore, in vivo activation of this pathway produced reward-related phenotypes that were dependent on intra-LHb $GABA_A$ receptor signaling. These results suggest that noncanonical inhibitory signaling by these hybrid dopaminergic-GABAergic neurons act to suppress LHb output under rewarding conditions.

INTRODUCTION

Dopaminergic neurons in the ventral tegmental area (VTA) are thought to encode reward prediction error—the difference between an expected reward and actual reward. Consistent with this, dopaminergic neurons are phasically excited by reward and the cues that predict them and are phasically inhibited by the omission of reward and aversive stimuli (Cohen et al., 2012; Matsumoto and Hikosaka, 2007; Pan et al., 2005; Schultz et al., 1997; Tobler et al., 2005; Ungless et al., 2004). Increased firing rate of dopaminergic neurons in response to salient stimuli causes phasic dopamine release in the nucleus accumbens (NAc), a signaling event thought to be critical for initiation of motivated behaviors (Day et al., 2007; Grace, 1991; Oleson et al., 2012; Phillips et al., 2003; Stuber et al., 2008).

The lateral habenula (LHb) is a key neuroanatomical regulator of midbrain reward circuitry. Although dopaminergic neurons are excited by rewarding stimuli and inhibited by the omission of reward, neurons in the LHb display contrary responses: they are inhibited by cues that predict reward and excited by the omission of reward (Matsumoto and Hikosaka, 2007). Importantly, in response to the omission of reward, excitation of the LHb neurons precedes the inhibition of dopaminergic neurons, suggesting that LHb neurons may modulate VTA dopaminergic neurons. Further supporting this claim, electrical stimulation of the LHb inhibits midbrain dopaminergic neurons (Christoph et al., 1986; Ji and Shepard, 2007), whereas pharmacological inhibition of the LHb increases dopamine release in the striatum (Lecourtier et al., 2008). Collectively, these data suggest that LHb neurons encode negative reward prediction errors and may negatively modulate midbrain dopaminergic neurons in response to aversive events.

The LHb sends a functional glutamatergic projection to the rostromedial tegmental nucleus (RMTg, also referred to as the tail of the VTA), a population of GABAergic neurons located posterior to the VTA (Brinschwitz et al., 2010; Jhou et al., 2009; Stamatakis and Stuber, 2012). In vivo activation of VTA-projecting LHb neurons (Lammel et al., 2012), or LHb glutamatergic terminals in the RMTg, produces aversion and promotes motivated behavior to avoid further activation of the LHb-to-RMTg pathway (Stamatakis and Stuber, 2012), demonstrating a causal role for this pathway in controlling aversive behavior. Because GABAergic RMTg neurons inhibit midbrain dopaminergic

neurons (Matsui and Williams, 2011), the RMTg is likely the intermediary structure through which the LHb inhibits midbrain dopaminergic neurons.

Although the LHb-to-midbrain circuit has been dissected both functionally and behaviorally, less is known about the importance of the various LHb afferents. Inputs to the LHb arise from forebrain regions including the lateral hypothalamus, entopenduncular nucleus (EN), and prefrontal cortex (Kim and Lee, 2012; Poller et al., 2013; Shabel et al., 2012; Warden et al., 2012). A recent study suggests that aversive signaling by the LHb is mediated in part from the EN, as in vivo activation of these afferents in the LHb is aversive (Shabel et al., 2012). Although the majority of LHb afferents arise from the forebrain, the LHb also receives a substantial projection from the VTA (Gruber et al., 2007; Phillipson and Griffith, 1980; Skagerberg et al., 1984), with an estimated 30%–50% of LHb-projecting VTA neurons being dopaminergic (Gruber et al., 2007; Skagerberg et al., 1984). Electrical stimulation of the midbrain decreases the firing rate of LHb neurons (Shen et al., 2012), but the functional and behavioral significance of synaptic inputs to the LHb arising from VTA dopaminergic neurons remains unknown. Here, we demonstrate that selective activation of this projection inhibits LHb neurons by the actions of synaptically released GABA, which disinhibits VTA dopaminergic neurons to promote reward-related behavior.

RESULTS

Optogenetic Targeting of VTA Dopaminergic Neurons and Innervation to the LHb

To selectively target VTA dopaminergic neurons, we introduced a Cre-inducible viral construct coding for channelrhodopsin-2 fused to an enhanced yellow fluorescent protein (ChR2-eYFP) bilaterally into the VTA of *tyrosine hydroxylase* (*TH*)-internal ribosome entry site-Cre (TH^{VTA}::ChR2) adult mice as previously described (Tsai et al., 2009). Three to four weeks following surgery, we observed robust ChR2-eYFP expression in the VTA (Figures 1A and 1B). To ensure the specificity of ChR2-eYFP for dopaminergic neurons, we quantified the number of VTA neurons that were TH-positive (TH^+) and eYFP-positive ($eYFP^+$). We found that 62.4% ± 3.4% of VTA neurons were TH^+, 48.6% ± 0.9% were $eYFP^+$, and 99.2% ± 0.4% of the $eYFP^+$ neurons were also labeled with TH (Figure 1C), consistent with previous results (Tsai et al., 2009). Six weeks following surgery, we observed eYFP expression that was largely restricted to the LHb relative to neighboring structures (Figures 1D and 1E). Fluorescence quantification analysis in brain slices containing the LHb revealed that axonal fibers originating from VTA dopaminergic neurons densely innervated the LHb, but only sparsely innervated surrounding structures, such as the medial habenula, thalamus, and hippocampus (Figure 1F).

LHb-Projecting VTA Dopaminergic Neurons Do Not Send Axon Collaterals to Other Reward-Related Brain Structures

We next determined whether LHb-projecting VTA dopaminergic neurons ($TH^{VTA\text{-}LHb}$) collateralize and project to other brain regions. To accomplish this, we utilized an intersectional genetic approach to selectively label TH^+ neurons in the VTA that project to the LHb. We bilaterally injected the LHb of *TH*-Cre mice with a retrogradely transducing herpes simplex virus (Chaudhury et al., 2013) encoding a Cre-inducible flippase recombinase (flp) under control the of an Ef1α promoter fragment (HSV-EF1α-LS1L-flp) (Figure S1 available online; see Supplemental Experimental Procedures for more detail) (Kuhlman and Huang, 2008). In the same surgery, we bilaterally injected a flp-inducible ChR2-eYFP (AAV5-EF1α-fdhChR2(H134R)-eYFP; a construct designed with the same structure as the Cre-inducible viral construct coding for ChR2 (Tsai et al., 2009) into the VTA (Figure 1G). This resulted in the selective labeling of the somas and processes of VTA TH^+ neurons that project to the LHb. If $TH^{VTA\text{-}LHb}$ neurons collateralize to other target regions, we would expect to see $eYFP^+$ fibers in these regions as well as the LHb. However, 6 weeks following this procedure, we observed $eYFP^+$ fibers in the LHb, but not in other terminal regions of VTA dopaminergic neurons, such as the medial prefrontal cortex (mPFC), NAc, basolateral amygdala (BLA), or bed nucleus of the stria terminalis (BNST) (Figures 1G and S1; n = 6 slices from n = 3 mice), suggesting that $TH^{VTA\text{-}LHb}$ neurons only project to the LHb and do not send collaterals to these other target structures. Additionally, in a separate group of *TH*-Cre mice, we bilaterally injected the HSV-EF1α-LS1L-flp virus into the NAc and the AAV5-EF1α-fdhChR2(H134R)-eYFP virus into the VTA. In these mice, we observed $eYFP^+$ fibers in the NAc, but not in the LHb (Figure S1, n = 6 slices from n = 3 mice).

$TH^{VTA\text{-}LHb}$ Neurons Are Distinct from $TH^{VTA\text{-}NAc}$ Neurons

To further confirm that $TH^{VTA\text{-}LHb}$ neurons are anatomically distinct from NAc-projecting VTA dopaminergic neurons ($TH^{VTA\text{-}NAc}$), and to provide an anatomical map of these discrete populations within the VTA, we performed retrograde tracing by injecting red fluorescent beads into the NAc and green fluorescent beads into the LHb of the same C57/BL6J wild-type mice (Figure 1H). Three weeks following surgery, VTA sections were collected and immunostained for TH. We found that $TH^{VTA\text{-}LHb}$ neurons were located in anterior and medial regions, congregating mainly in the interfasicular nucleus, whereas $TH^{VTA\text{-}NAc}$ neurons were generally located more posterior and lateral (Figure 1I). Additionally, we observed significantly more $TH^{VTA\text{-}NAc}$ neurons than $TH^{VTA\text{-}LHb}$ neurons throughout the VTA (Figure 1I). Supporting our viral tracing data, we detected no TH^+ neurons that expressed both red and green retrobeads in the VTA. Collectively, these data demonstrate that $TH^{VTA\text{-}LHb}$ and $TH^{VTA\text{-}NAc}$ neurons are completely separate neuronal populations.

Because we found that $TH^{VTA\text{-}NAc}$ and $TH^{VTA\text{-}LHb}$ neurons are separate populations of neurons within the VTA, we investigated whether these two populations display different electrophysiological characteristics. To accomplish this, we injected two groups of *TH*-GFP mice with red retrobeads either in the NAc or LHb and performed whole-cell recordings from GFP-positive neurons in VTA brain slices containing retrobeads (Figure 2A). Unlike $TH^{VTA\text{-}NAc}$ neurons, $TH^{VTA\text{-}LHb}$ neurons did not show a hyperpolarization-activated inward rectifying current (I_h), a traditional (although disputed) marker of midbrain dopaminergic

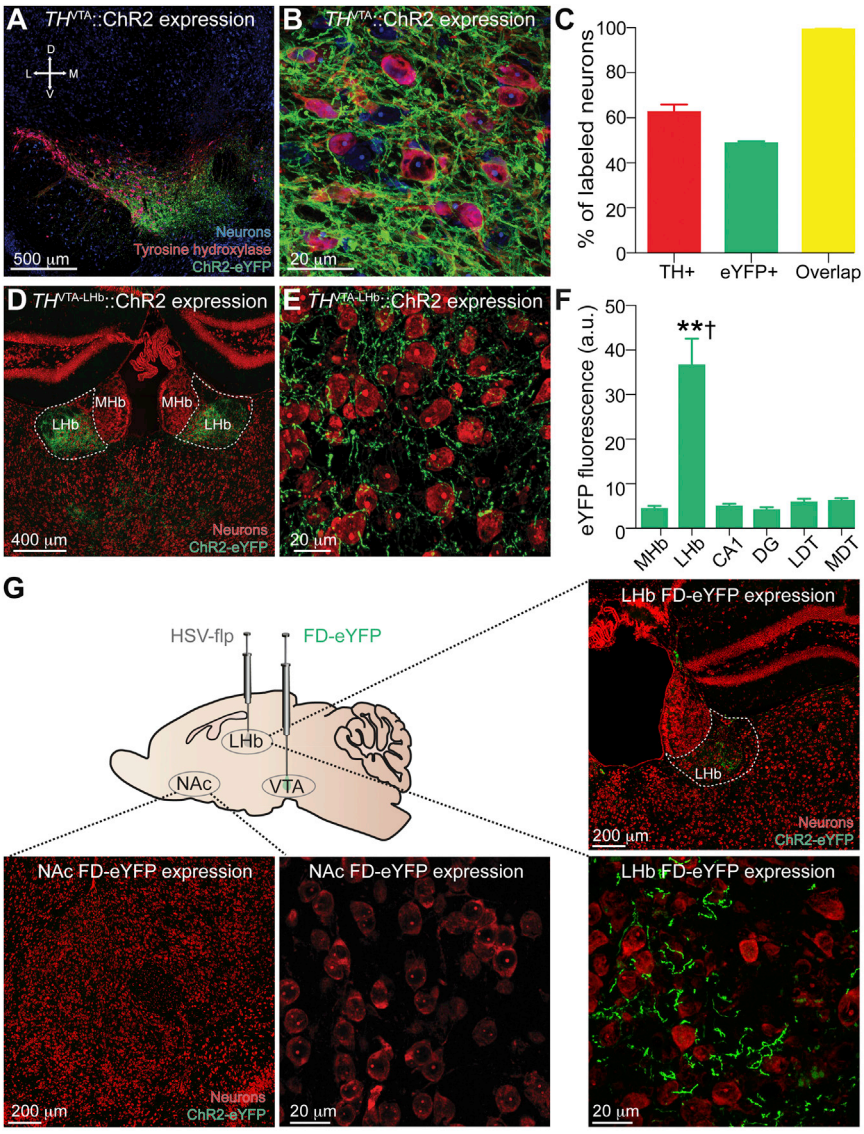

Figure 1. $TH^{VTA\text{-}LHb}$ Neurons Are a Distinct Population of Neurons

(A and B) Confocal images of coronal sections showing expression of ChR2-eYFP in the VTA following injection of Cre-inducible virus into the VTA of a *TH*-IRES-Cre (TH^{VTA}::ChR2) mouse.

(C) Quantification of TH^+, $eYFP^+$, and $eYFP^+$ neurons that are also TH^+ (n = 4 sections from n = 3 mice).

(D and E) Confocal images of coronal sections showing expression of ChR2-eYFP fibers in the LHb of a TH^{VTA}::ChR2 mouse.

(F) eYFP fluorescence intensity is significantly higher in the LHb than in surrounding regions ($F[5,30] = 5.718$, $p < 0.0001$; n = 6 sections from n = 3 mice). MHb, medial habenula; LHb, lateral habenula; DG, dentate gyrus; LDT, lateral dorsal thalamus; MDT, medial dorsal thalamus.

(G) Diagram illustrates HSV-EF1α-LS1L-flp (HSV-flp) and AAV5-EF1α-fdhChR2(H134R)-eYFP (FD-eYFP) viral injections. Confocal images show eYFP expression in the NAc (below) and LHb (right) following injection of HSV-flp into the LHb and FD-eYFP into the VTA of *TH*:IRES:Cre mice. See also Figure S1.

(H) Left: schematic of retrobead injections. Right: confocal images of separate TH^+ neurons containing NAc-injected beads (top) and LHb-injected beads (bottom).

(I) Left: location of $TH^{VTA\text{-}NAc}$ neurons (red) and $TH^{VTA\text{-}LHb}$ neurons (green) from a representative animal. Right: more TH^+ neurons in the VTA contained red retrobeads ($TH^{VTA\text{-}NAc}$ neurons) than green retrobeads ($TH^{VTA\text{-}LHb}$ neurons) (anterior: $t[8] = 3.01$, $p = 0.02$; n = 5 sections from n = 4 mice; middle: $t[8] = 6.51$, $p = 0.0002$; n = 5 sections from n = 4 mice; posterior: $t[6] = 9.58$, $p < 0.0001$; n = 4 sections from n = 4 mice). Error bars represent SEM. **$p < 0.01$ (Student's t test and ANOVA followed by Bonferroni post hoc comparisons, where applicable). Dagger symbol denotes significance compared to all manipulations.

neurons (Margolis et al., 2006; Mercuri et al., 1995) (Figure 2B). The lack of I_h, together with increased membrane resistance (Figure 2C), suggests that $TH^{VTA\text{-}LHb}$ neurons may be more excitable than $TH^{VTA\text{-}NAc}$ neurons. Supporting this observation, we found that $TH^{VTA\text{-}LHb}$ neurons show enhanced spontaneous activity compared to $TH^{VTA\text{-}NAc}$ neurons (Figures 2D and 2E).

A pharmacological signature of midbrain dopaminergic neurons is their hyperpolarization in response to D2 autoreceptor activation (Beckstead et al., 2004). To determine whether $TH^{VTA\text{-}LHb}$ neurons are sensitive to D2 autoreceptor activation, we performed cell-attached recordings from $TH^{VTA\text{-}LHb}$ and $TH^{VTA\text{-}NAc}$ neurons in the VTA. In line with previous data, we observed a significant decrease in spontaneous firing following a D2 receptor agonist (3 μM quinpirole) bath application in $TH^{VTA\text{-}NAc}$ neurons (Figures 2D, 2F; Beckstead et al., 2004; Lammel et al.,

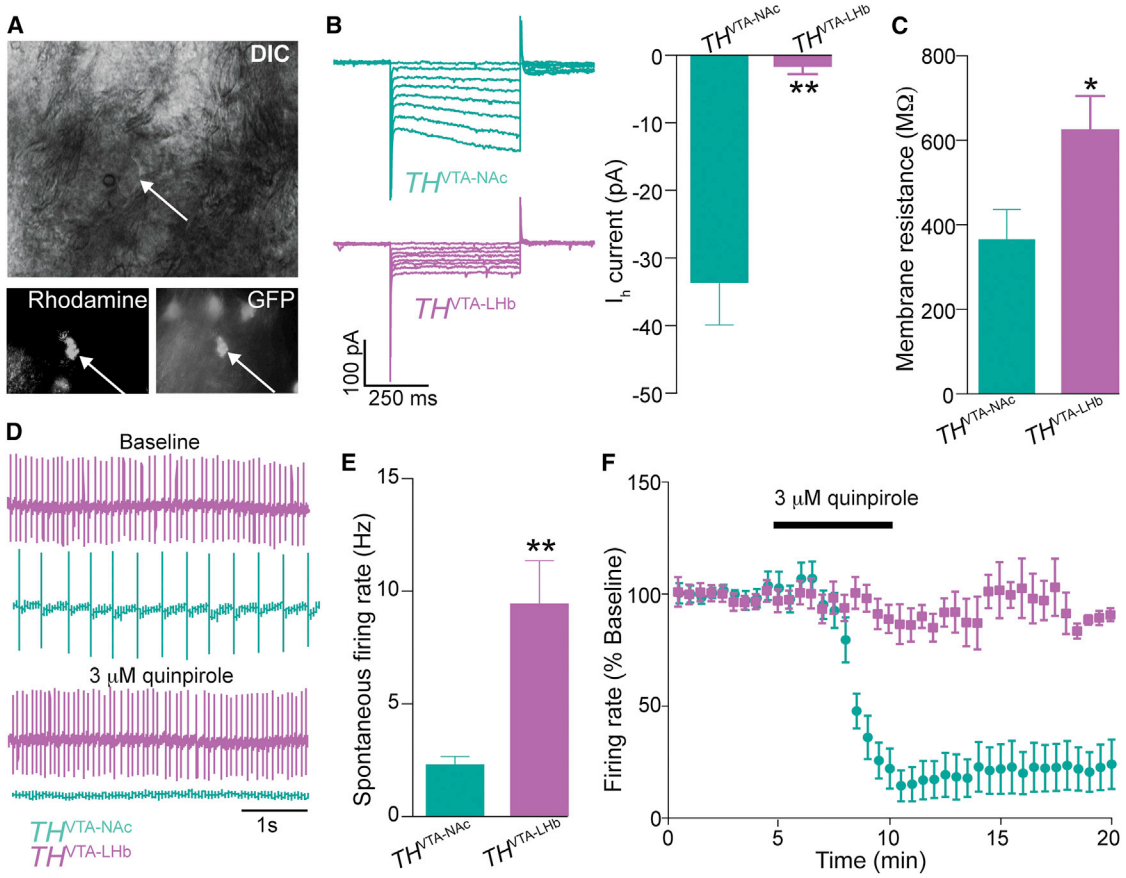

Figure 2. *TH*$^{VTA-LHb}$ Neurons Exhibit Distinct Electrophysiological Characteristics

(A) Top: VTA neuron (indicated by arrow) visualized with a DIC microscope. Bottom left: same neuron visualized under epifluorescent illumination with rhodamine filter. Bottom right: same neuron visualized under epifluorescent illumination with GFP filter.

(B) Left: representative traces showing I_h current in a *TH*$^{VTA-NAc}$ neuron (top) and *TH*$^{VTA-LHb}$ neuron (bottom) in response to voltage steps. Right: *TH*$^{VTA-LHb}$ neurons show significantly less I_h current than *TH*$^{VTA-NAc}$ neurons ($t[16] = 4.5$, $p = 0.0004$; n = 10 *TH*$^{VTA-NAc}$ neurons and 8 *TH*$^{VTA-LHb}$ neurons).

(C) *TH*$^{VTA-LHb}$ neurons have a higher membrane resistance than *TH*$^{VTA-NAc}$ neurons ($t[16] = 2.4$, $p = 0.03$; n = 10 *TH*$^{VTA-NAc}$ neurons and 8 *TH*$^{VTA-LHb}$ neurons).

(D) Representative traces showing spontaneous firing of *TH*$^{VTA-LHb}$ neuron (purple) and *TH*$^{VTA-NAc}$ neuron (green) during a baseline period (top) and following a bath application of a D2 agonist (3 μM quinpirole, bottom).

(E) Spontaneous firing is significantly higher in *TH*$^{VTA-LHb}$ neurons than in *TH*$^{VTA-NAc}$ neurons ($t[17] = 3.78$, $p = 0.0015$; n = 10 *TH*$^{VTA-NAc}$ neurons and 9 *TH*$^{VTA-LHb}$ neurons).

(F) Bath application (3 μM) of quinpirole decreases the spontaneous firing rate significantly more for *TH*$^{VTA-NAc}$ neurons compared to *TH*$^{VTA-LHb}$ neurons ($F[34,490] = 10.58$, $p = < 0.0001$; n = 9 *TH*$^{VTA-NAc}$ neurons and 7 *TH*$^{VTA-LHb}$ neurons. Error bars represent SEM. *$p < 0.05$ **$p < 0.01$ (Student's t test and ANOVA followed by Bonferroni post hoc comparisons, where applicable).

2008). However, quinpirole did not significantly change the spontaneous firing rate of *TH*$^{VTA-LHb}$ neurons (Figures 2D, 2F), demonstrating that *TH*$^{VTA-LHb}$ neurons lack functional somatodendritic D2 autoreceptors.

Because *TH*$^{VTA-LHb}$ and *TH*$^{VTA-NAc}$ neurons are anatomically and electrophysiologically distinct, we quantified the gene expression profiles of these two populations. To characterize the molecular phenotype of *TH*$^{VTA-LHb}$ and *TH*$^{VTA-NAc}$ neurons, we injected two groups of TH-GFP mice with red retrobeads either in the NAc or LHb and 7 days later extracted the intracellular contents from individual GFP-positive neurons in VTA brain slices containing retrobeads (Figure 3A). The intracellular content was then processed by reverse transcription quantitative PCR assaying the following genes: vesicular glutamate transporter-2 (*Vglut2*), vesicular GABA transporter (*Vgat*), glutamate decarboxylase 1 and 2 (*GAD1*/*GAD2*), vesicular monoamine transporter-2 (*Vmat2*), dopamine receptor D2 (*DRD2*), dopamine transporter (*DAT1*), and tyrosine hydroxylase (*TH*). We found that both *TH*$^{VTA-LHb}$ and *TH*$^{VTA-NAc}$ neurons expressed all tested genes classically associated with dopamine synthesis, release, and uptake (*Vmat2*, *DRD2*, *DAT1*, and *TH*; Figure 3B). However, *TH*$^{VTA-LHb}$ neurons expressed significantly lower amounts of *Vmat2*, *DRD2*, and *DAT1* compared to *TH*$^{VTA-NAc}$ neurons (Figure 3C). Importantly, none of these dopaminergic markers were detected in GFP-negative neurons (n = 7 neurons). Taken together, these data suggest that *TH*$^{VTA-LHb}$ neurons are anatomically, electrophysiologically, and genetically distinct from *TH*$^{VTA-NAc}$ neurons.

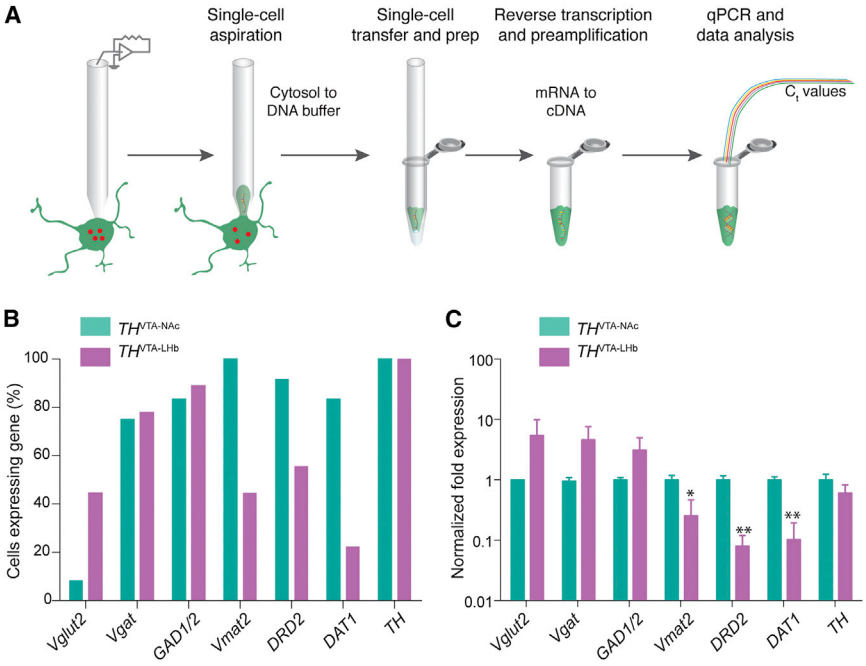

Figure 3. $TH^{VTA\text{-}LHb}$ Neurons Express Lower Amounts of mRNA for Dopaminergic Markers than $TH^{VTA\text{-}NAc}$ Neurons

(A) Schematic of single-cell RT-PCR analysis.

(B) Percentage of $TH^{VTA\text{-}LHb}$ and $TH^{VTA\text{-}NAc}$ neurons expressing each gene (*Vglut2*, vesicular glutamate transporter-2; *Vgat,* vesicular GABA transporter; *GAD1/GAD2,* glutamate decarboxylase 1 and 2; *Vmat2*, vesicular monoamine transporter-2; *DRD2,* dopamine receptor D2; *DAT1*, dopamine transporter; and *TH,* tyrosine hydroxylase).

(C) C_t values for each target gene were normalized to the control gene expressed in all neurons, *Rn18s*, and log transformed fold expression values represent single cell expression relative to $TH^{VTA\text{-}NAc}$ expression. The average fold expression for *Vmat2*, *DRD2*, and *DAT1* is significantly lower in $TH^{VTA\text{-}LHb}$ neurons compared $TH^{VTA\text{-}NAc}$ neurons (*Vmat2*: U = 19, p = 0.0136; *DRD2*: U = 10, p = 0.0053; *DAT1*: U = 17.00, p = 0.0069; n = 9 $TH^{VTA\text{-}LHb}$ neurons from n = 4 mice and n = 12 $TH^{VTA\text{-}NAc}$ neurons from n = 3 mice). Error bars represent SEM. *p < 0.05 **p < 0.01 (Mann-Whitney).

Characterization of Neurotransmitter Release from $TH^{VTA\text{-}LHb}$ Fibers

To characterize the dynamics of dopamine release from synaptic fibers that innervate the LHb, we performed fast-scan cyclic voltammetry in LHb brain slices obtained from TH^{VTA}::ChR2 mice. Carbon-fiber microelectrodes were placed in areas within the LHb that displayed the highest ChR2-eYFP expression to ensure the voltammetry electrodes were near presynaptic fibers and synapses that could be optically stimulated. We observed no detectable optically evoked dopamine release within the LHb, even after sustained high-frequency optical stimulation (Figures 4A–4C). As positive controls, we recorded light-evoked dopamine release in NAc and BNST brain slices obtained from the same TH^{VTA}::ChR2 mouse. We observed robust light-evoked dopamine release that increased as a function of either frequency or pulse number in both the NAc and BNST (Figures 4A–4C), consistent with previous studies in the NAc and dorsal striatum of rats (Bass et al., 2013; Witten et al., 2011). We were unable to detect dopamine release in the LHb even after altering the parameters of the voltammetry experiments to increase the sensitivity of dopamine detection (Figure S2; see Experimental Procedures for additional details). Fluorescence quantification analysis of TH^{VTA}::ChR2 fibers in the NAc, BNST, and LHb revealed that although the NAc had significantly higher eYFP fluorescence, there was no difference in eYFP intensity between the LHb and BNST (Figures 4D and 4E). These data suggest that the lack of detectable dopamine release in LHb brain slices is not likely due to weaker innervation, as we observed optically-evoked dopamine release in BNST slices that show comparable innervation.

In the NAc and BNST, we also observed intense TH immunofluorescence and a high degree of colocalization between $eYFP^+$ fibers and TH immunostaining (Figures 4D and 4F) in brain slices obtained from TH^{VTA}::ChR2 mice. In contrast, the LHb from the same mice exhibited strong eYFP fluorescence, but almost no TH immunoreactivity (Figures 4D and 4F). Quantitative analysis confirmed that colocalization (as assessed by Pearson's correlation coefficient) between eYFP and TH was 0.52 ± 0.05 for NAc and 0.50 ± 0.04 for the BNST, but only 0.010 ± 0.004 for the LHb. Together, these data suggest that fibers arising from VTA TH^+ neurons express little or no TH in the fibers that innervate the LHb.

Because we did not observe dopamine release in the LHb, we sought to determine whether this projection might release other neurotransmitters in the LHb. In light of recent studies demonstrating that dopaminergic fibers can corelease glutamate and GABA in the striatum (Stuber et al., 2010; Tecuapetla et al., 2010; Tritsch et al., 2012), we asked whether fibers and synapses originating from TH^{VTA} neurons were capable of releasing either of these neurotransmitters in the LHb. Accordingly, we performed whole-cell voltage-clamped recordings from postsynaptic LHb neurons in brain slices obtained from TH^{VTA}::ChR2 mice. To ensure we were only recording monosynaptic currents from TH^{VTA}::ChR2 fibers, we added a Na^+-channel blocker (1 μM TTX) and a K^+-channel blocker (1 mM 4-AP) to the bath as previously described (Cruikshank et al., 2010). Voltage-clamp recordings from LHb neurons revealed that light pulses that selectively stimulated TH^{VTA}::ChR2 fibers in the LHb ($TH^{VTA\text{-}LHb}$::ChR2), produced light-evoked currents that were blocked by 10 μM of the $GABA_A$ receptor antagonist gabazine (Figures 5A–5C). Of the neurons we recorded from in the LHb, 82% (45/55) received a direct monosynaptic inhibitory input from TH^{VTA} neurons. Dopaminergic terminals in the dorsal striatum release GABA that is dependent on *Vmat2* activity (Tritsch et al., 2012). However, we observed no changes in inhibitory currents in LHb slices from TH^{VTA}::ChR2 mice treated with the *Vmat2* inhibitor reserpine, compared to untreated slices (Figure 5D). This same reserpine protocol was sufficient to inhibit

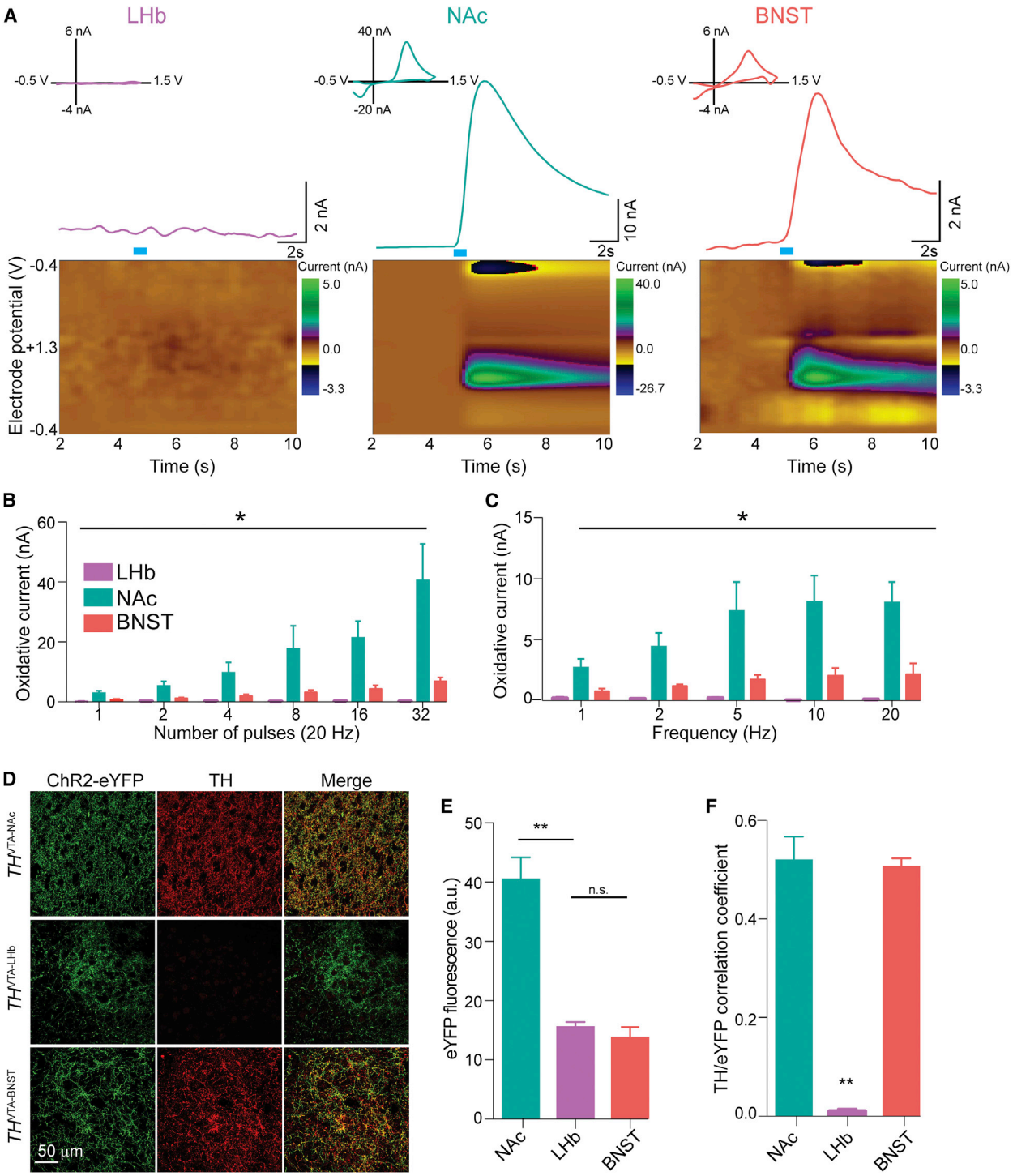

Figure 4. $TH^{VTA\text{-}LHb}$ Neurons Do Not Release Detectable Levels of Dopamine in the LHb

(A) Fast-scan cyclic voltammetric recordings of optically-evoked dopamine release in LHb (left), NAc (middle), and BNST (right) brain slices from TH^{VTA}::ChR2 mice. Top: example traces of voltammetric recordings from LHb (left), NAc (middle), and BNST (right) brain slices. Insets: background-subtracted cyclic voltammograms showing an electrochemical signal indicative of oxidized dopamine in the NAc and BNST, but not in the LHb. Bottom: consecutive background-subtracted voltammograms recorded over the 8 s interval. Applied potential (E_{apps} versus Ag/AgCl reference electrode) is shown on y axis. Time at which each voltammogram was recorded is shown on x axis. Current changes are color-coded.

(B) Light-evoked current is significantly higher in the NAc than LHb at 20 Hz for all measured number of pulses ($F[5,1] = 19.1$, $p < 0.0001$). Light-evoked current is significantly higher in the BSNT than LHb at 20 Hz for 8, 16, and 32 pulses ($F[5,1] = 72.59$, $p < 0.0001$).

(legend continued on next page)

electrically-evoked dopamine release in the NAc (Figure S3), demonstrating that this treatment was capable of inhibiting *Vmat2* and depleting evoked dopamine. These data demonstrate that $TH^{VTA\text{-}LHb}$ neurons do not require *Vmat2* function to release GABA in the LHb. Additionally, we observed a small (−7.2 ± 2.2 pA) excitatory current in some of the recorded neurons (5/10), consistent with a previous study demonstrating that *Vglut2*-expressing VTA neurons (some of which could be dopaminergic) innervate the LHb (Hnasko et al., 2012).

To determine whether activating $TH^{VTA\text{-}LHb}$::ChR2 terminals would affect the spontaneous firing rate of postsynaptic LHb neurons, we performed cell-attached recordings from LHb neurons and found that the average spontaneous firing rate of these neurons was 8.0 ± 2.2 Hz. When we delivered a 1 s 20 Hz optical pulse-train to optically stimulate $TH^{VTA\text{-}LHb}$::ChR2 terminals, we observed that the firing rate of LHb neurons significantly decreased (Figures 5E–5G), demonstrating that the net effect of $TH^{VTA\text{-}LHb}$::ChR2 terminal stimulation was to suppress the firing of LHb neurons. To determine whether this suppression of firing was due to GABA or dopamine release, we added a D1/D2 receptor antagonist cocktail (10 μM SCH23390 and 10 μM raclopride) to the bath, followed by a $GABA_A$ receptor antagonist (10 μM gabazine). The D1/D2 receptor antagonist did not modify the decrease in firing in response to optical stimulation, but the $GABA_A$ receptor antagonist blocked this decrease, leading us to conclude that the inhibition of spontaneous firing following activation of $TH^{VTA\text{-}LHb}$::ChR2 terminals is due to activation of $GABA_A$ receptors.

We performed electron microscopy to provide anatomical support for the electrophysiological findings. Accordingly, we collected images of $TH^{VTA\text{-}LHb}$::ChR2 synapses (as defined by electron-dense DAB reaction product or silver-enhanced nanogold after pre-embedding immunostaining for eYFP). Postembedding immunogold staining performed on this material showed that many of these presynaptic terminals contained high levels of GABA (Figure 5H). In some cases we also saw terminals containing little or no GABA that made asymmetric synaptic contacts (Figure S4); these were likely to be glutamatergic. Collectively, these congruous findings demonstrate that $TH^{VTA\text{-}LHb}$::ChR2 terminals do not release detectable amounts of dopamine in the LHb in an impulse-dependent fashion. Instead, $TH^{VTA\text{-}LHb}$::ChR2 projections contain and release GABA, which functions to suppress the activity of postsynaptic LHb neurons.

The Functional Significance of the $TH^{VTA\text{-}LHb}$ Circuit in Regulating Midbrain Activity

Because the inhibitory $TH^{VTA\text{-}LHb}$ pathway suppresses the activity of postsynaptic LHb neurons (Figures 5E–5G), we next addressed whether activation of this inhibitory circuit has downstream effects on midbrain activity in vivo. Given that the LHb sends a strong glutamatergic projection to the RMTg (Stamatakis and Stuber, 2012), we assessed the functional consequences of $TH^{VTA\text{-}LHb}$ activation on RMTg neuronal activity by recording extracellularly from RMTg neurons in anesthetized mice while stimulating $TH^{VTA\text{-}LHb}$ terminals (Figure 6A). Optical stimulation of the $TH^{VTA\text{-}LHb}$ pathway suppressed the spontaneous firing of RMTg neurons (Figures 6B and 6C). Further, these recorded RMTg units did not respond to optical stimulation within the RMTg (Figure S5), confirming that the recorded neurons did not express ChR2-eYFP. In agreement with this, we observed minimal ChR2-eYFP and TH^+ immunolabeling in RMTg brain slices (Figure S5). Therefore, we considered these neurons to be *TH*-negative neurons, consistent with previous data (Barrot et al., 2012).

Because RMTg neurons directly inhibit VTA dopaminergic (TH^{VTA}) neurons (Matsui and Williams, 2011), we next determined if optical stimulation of $TH^{VTA\text{-}LHb}$ terminals would enhance TH^{VTA} neuronal activity via disinhibition. First, to optically classify recorded units as TH^{VTA} neurons, we recorded the firing responses of VTA neurons to the delivery of 2 ms light pulses within the VTA (Figures 6D and 6E). Optically identified TH^{VTA} neurons displayed time-locked activation to VTA optical stimulation (Figures 6E and 6F).

Following identification of TH^{VTA} neurons, we determined whether optical stimulation of the $TH^{VTA\text{-}LHb}$ inhibitory pathway (by delivering 473 nm light directly into the LHb) could alter the spontaneous activity of TH^{VTA} neurons. Optical stimulation of $TH^{VTA\text{-}LHb}$ terminals led to enhanced spontaneous activity in optically identified TH^{VTA} neurons (Figures 6G and 6H). Importantly, we determined that these light-evoked responses were unlikely to arise from antidromic activation of $TH^{VTA\text{-}LHb}$ terminals, as $TH^{VTA\text{-}LHb}$ initiated spikes had significantly longer spike latencies and greater spike jitter compared to the light-evoked spikes of TH^{VTA} neurons with direct optical stimulation in the VTA (Figure 6I). Furthermore, TH^{VTA} neurons did not respond reliably to 20 Hz optical stimulation of $TH^{VTA\text{-}LHb}$ terminals (Figure 6J). Collectively, these data suggest that the increases in firing of TH^{VTA} neurons initiated by $TH^{VTA\text{-}LHb}$ terminal activation are mediated through synaptic transmission within a polysynaptic circuit. Taken together, these circuit-activity mapping experiments reveal the functional significance of the inhibitory $TH^{VTA\text{-}LHb}$ pathway in regulating midbrain activity.

Optogenetic Activation of the $TH^{VTA\text{-}LHb}$ Pathway Produces Reward-Related Behavioral Phenotypes that Require $GABA_A$ Signaling

In vivo, pharmacological inhibition of the LHb increases dopamine in forebrain regions such as the striatum (Lecourtier et al., 2008). Likewise, we observed that in vivo activation of the

(C) Light-evoked current is significantly higher in the NAc than LHb for all measured frequencies ($F[4,1] = 29.11$, $p < 0.001$). Light-evoked current is significantly higher in the BNST than LHb for 10 and 20 Hz ($F[4,1] = 25.43$, $p < 0.001$). See also Figure S2.
(D) Confocal images showing eYFP- and TH-expression in the NAc (top), LHb (middle), and BNST (bottom) from TH^{VTA}::ChR2 coronal sections.
(E) eYFP fluorescence intensity is significantly higher in the NAc than in the LHb ($t[10] = 6.58$, $p < 0.0001$). eYFP fluorescence intensity is not significantly different between the LHb and BNST ($t[10) = 0.9002$, $p = 0.389$). n = 6 slices/region from n = 3 mice.
(F) ChR2-eYFP and TH colocalize significantly less in the LHb than in the BNST and NAc (Pearson's correlation coefficient, $F[2,12] = 76.49$, $p < 0.0001$; n = 5 slices/region from n = 3 mice). Error bars represent SEM. **$p < 0.01$ (Student's t test and ANOVA followed by Bonferroni post hoc comparisons, where applicable).

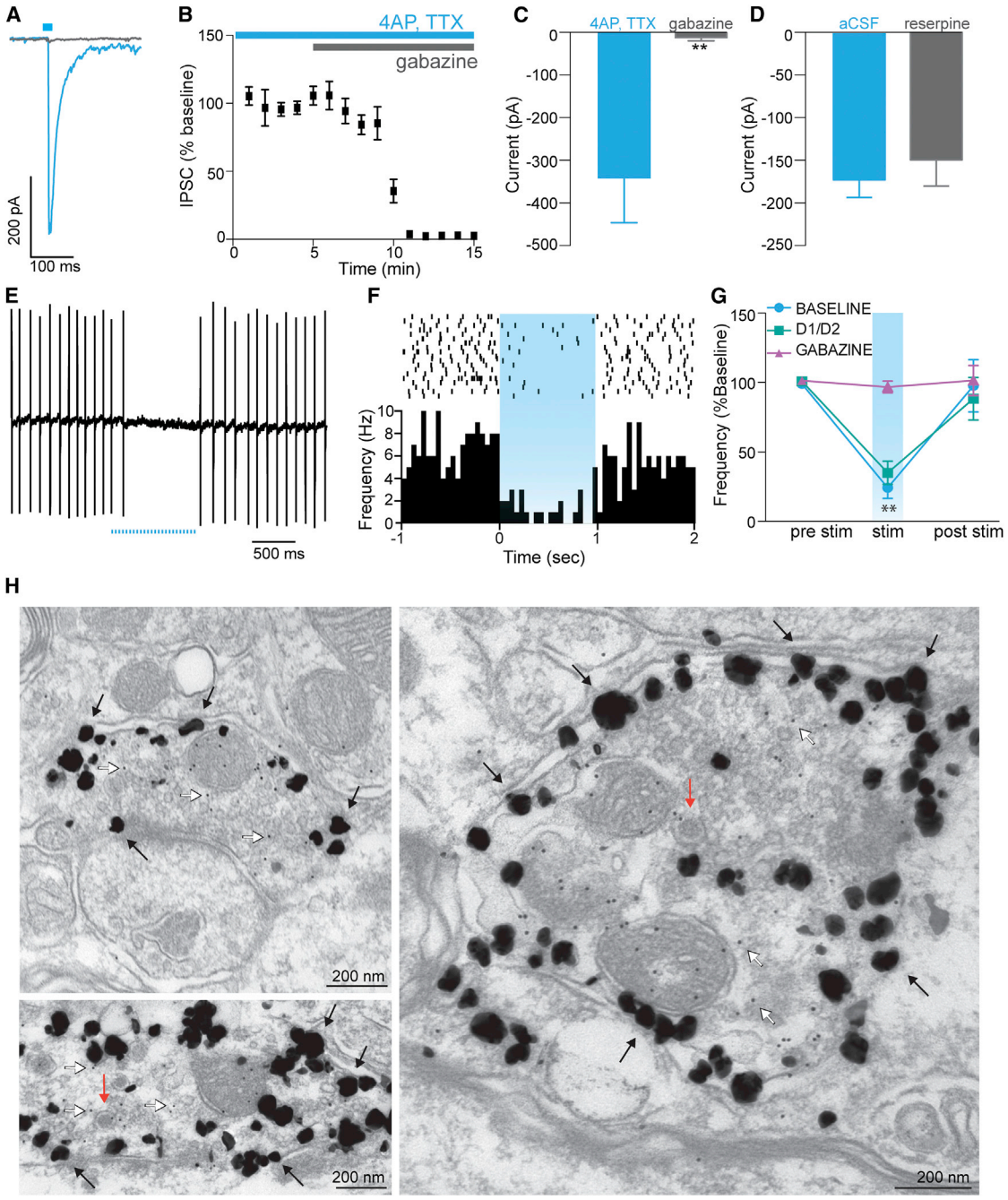

Figure 5. *TH*$^{VTA-LHb}$ Neurons Release GABA in the LHb

(A–C) Light-evoked IPSCs recorded from LHb neurons in the presence of 1 mM 4-AP and 1 μM TTX are blocked by bath-application of 10 μM gabazine ($t(12) = 3.12$, $p = 0.009$; $n = 7$ neurons).

(D) Light-evoked IPSCs recorded from LHb neurons in normal aCSF and from reserpine-treated mice ($t[18] = 0.60$; $p = 0.56$; $n = 10$ neurons each). See also Figure S3.

(E–G) Cell-attached recordings demonstrating a significant decrease in the spontaneous firing rate of LHb neurons in response to a 1 s 20 Hz optical stimulation of *TH*$^{VTA-LHb}$::ChR2 terminals in the LHb in normal aCSF (baseline: $t[14] = 9.57$, $p < 0.0001$) and after application of a D1/D2 antagonist (D1/D2: $t[14] = 7.76$, $p < 0.0001$), but not after application of a $GABA_A$ receptor antagonist (gabazine: $t[14] = 1.05$, $p = 0.31$) $n = 10$ neurons.

(H) Electron micrographs showing *TH*$^{VTA-LHb}$::ChR2 fibers, as defined by large silver-enhanced nanogold particles (black arrows) containing GABA (detected with 10 nm gold particles, white arrows). *TH*$^{VTA-LHb}$::ChR2 fibers also contain dense-core vesicles (red arrows). See also Figure S4. Error bars represent SEM. **$p < 0.01$ (Student's t test and ANOVA followed by Bonferroni post hoc comparisons, where applicable).

$TH^{VTA\text{-}LHb}$ pathway increased the firing rate of midbrain dopaminergic neurons (Figure 6). Therefore, we hypothesized that in vivo activation of the $TH^{VTA\text{-}LHb}$::ChR2 pathway would result in a reward-related phenotype. To test this hypothesis, we implanted bilateral optical fibers (Sparta et al., 2012) aimed directly above the LHb in $TH^{VTA\text{-}LHb}$::ChR2 mice (Figure S6) and determined the behavioral ramifications of selectively activating the $TH^{VTA\text{-}LHb}$::ChR2 pathway. Using a real-time place preference assay, as previously described (Stamatakis and Stuber, 2012), $TH^{VTA\text{-}LHb}$::ChR2 mice exhibited a significant preference for the side of the chamber that was paired with optical stimulation. In contrast, littermate controls ($TH^{VTA\text{-}LHb}$::Control) displayed no preference, demonstrating that activation of the $TH^{VTA\text{-}LHb}$::ChR2 pathway produces reward-related behaviors (Figures 7A–7C). This preference was dependent on $GABA_A$ signaling within the LHb, as intra-LHb microinjections of a $GABA_A$ receptor antagonist (gabazine) through guide cannulas interfaced with the optical fibers (Jennings et al., 2013) blocked the preference for the stimulation-paired side (Figures 7D and S7). In contrast, intra-LHb microinjection of a dopamine receptor antagonist (D1 and D2) cocktail did not block the rewarding phenotype (Figures 7D and S7), whereas a systemic injection of the dopamine antagonist cocktail did disrupt the preference (Figures 7E and S7). These data suggest that the observed reward-related phenotype induced by optical stimulation of the $TH^{VTA\text{-}LHb}$::ChR2 pathway does not depend on dopamine signaling within the LHb, but rather on downstream dopamine signaling in brain regions such as the NAc. Finally, to determine if activation of the $TH^{VTA\text{-}LHb}$::ChR2 pathway is reinforcing, we trained mice to nose-poke for optical stimulation of the $TH^{VTA\text{-}LHb}$::ChR2 pathway (Figures 7F–7H). $TH^{VTA\text{-}LHb}$::ChR2 mice made significantly more nose-pokes to receive optical stimulation than $TH^{VTA\text{-}LHb}$::control mice (Figure 7F).

Taken together, these data demonstrate that although activation of $TH^{VTA\text{-}LHb}$::ChR2 terminals does not result in detectable dopamine release in the LHb, selective activation of this pathway promotes reward-related behavior by suppressing LHb activity through the release of GABA, leading to disinhibition of VTA dopaminergic neurons.

DISCUSSION

Aberrant mesolimbic and mesocortical dopaminergic signaling has been implicated in a range of neuropsychiatric diseases, including schizophrenia, addiction, and depression (Chaudhury et al., 2013; Knable and Weinberger, 1997; Lüscher and Malenka, 2011; Phillips et al., 2003; Tye et al., 2013), motivating extensive studies of VTA dopaminergic projections to the striatum and prefrontal cortex. In contrast, little is known about the VTA's projection to the LHb. Using optogenetics in combination with electrophysiology, genetically targeted neuronal tracing techniques, and behavior, we investigated the functional and behavioral significance of this mesohabenular pathway.

Previous studies have demonstrated that separate populations of VTA dopaminergic neurons project to nonoverlapping target structures such as the NAc, BLA, and mPFC (Ford et al., 2006; Lammel et al., 2008; Swanson, 1982). Our data are consistent with these findings, demonstrating that $TH^{VTA\text{-}LHb}$ neurons do not collateralize to the NAc, BLA, PFC, or BNST. We also found that $TH^{VTA\text{-}LHb}$ neurons display electrophysiological characteristics distinct from $TH^{VTA\text{-}NAc}$ neurons. Notably, we found that $TH^{VTA\text{-}LHb}$ neurons are more excitable than $TH^{VTA\text{-}NAc}$ neurons, are insensitive to D2 autoreceptor activation, and do not display an I_h current, an electrophysiological characteristic often used to identify a neuron as dopaminergic in slice electrophysiological experiments (Mercuri et al., 1995). Recent studies have demonstrated that although NAc-projecting and BLA-projecting VTA dopaminergic neurons typically have robust I_h currents, dopaminergic neurons that project to the mPFC lack I_h currents and functional somatodendritic D2 autoreceptors (Ford et al., 2006; Lammel et al., 2008, 2011). Collectively, these data support the idea that VTA dopaminergic neurons are not a homogenous population, as they can vary greatly depending on their electrophysiological markers and their projection targets.

Although $TH^{VTA\text{-}LHb}$ neurons express TH mRNA and show TH immunostaining in the soma (Figures 1H and 3), we observed only very weak TH expression in $TH^{VTA\text{-}LHb}$::ChR2 fibers and terminals (Figure 4D). Consistent with this, voltammetric methods failed to detect released dopamine in the LHb following optical stimulation of $TH^{VTA\text{-}LHb}$::ChR2 fibers. It is worth noting that we observed dense core vesicles in presynaptic terminals originating from $TH^{VTA\text{-}LHb}$ neurons (Figure 5H). Previous work has demonstrated that the vesicular monoamine transporter can be associated with dense core vesicles in VTA neurons, suggesting that dopamine may be contained in both clear synaptic vesicles and dense core vesicles (Nirenberg et al., 1996). It is possible that a low content of dopamine within the dense core vesicles in the LHb could be released following specific stimulation patterns, leading to concentrations of dopamine in the LHb too low to detect with voltammetric methods. Additionally, because TH is produced in the soma, $TH^{VTA\text{-}LHb}$ neurons may be releasing dopamine locally from the somatodendritic compartment, which could then activate D2 autoreceptors to modulate the firing rate of neighboring VTA neurons (Adell and Artigas, 2004).

Previous studies have found that systemic injections of dopaminergic agonists and bath-application of high concentrations of dopamine result in changes in the firing patterns and glucose utilization of LHb neurons (Jhou et al., 2013; Kowski et al., 2009; McCulloch et al., 1980). However, as dopaminergic agonists often have affinities for serotonin receptors (Newman-Tancredi et al., 2002), which are thought to reside on presynaptic terminals in the LHb (Shabel et al., 2012), it is unclear whether the effects of these agonists on LHb activity arise from direct activation of dopamine receptors in the LHb.

LHb neurons exhibit a high basal firing rate both in slices (Figure 5; Jhou et al., 2013) and in vivo (Bromberg-Martin et al., 2010; Meier and Herrling, 1993), which likely exerts a tonic inhibitory influence on dopaminergic neurons by activating RMTg GABAergic neurons that directly inhibit VTA dopaminergic neurons. Supporting this hypothesis, we found that inhibition of LHb neurons through activation of $TH^{VTA\text{-}LHb}$::ChR2 terminals decreased RMTg firing and increased the spontaneous firing rate of VTA dopaminergic neurons (Figure 6), consistent with previous data demonstrating that pharmacological inhibition of

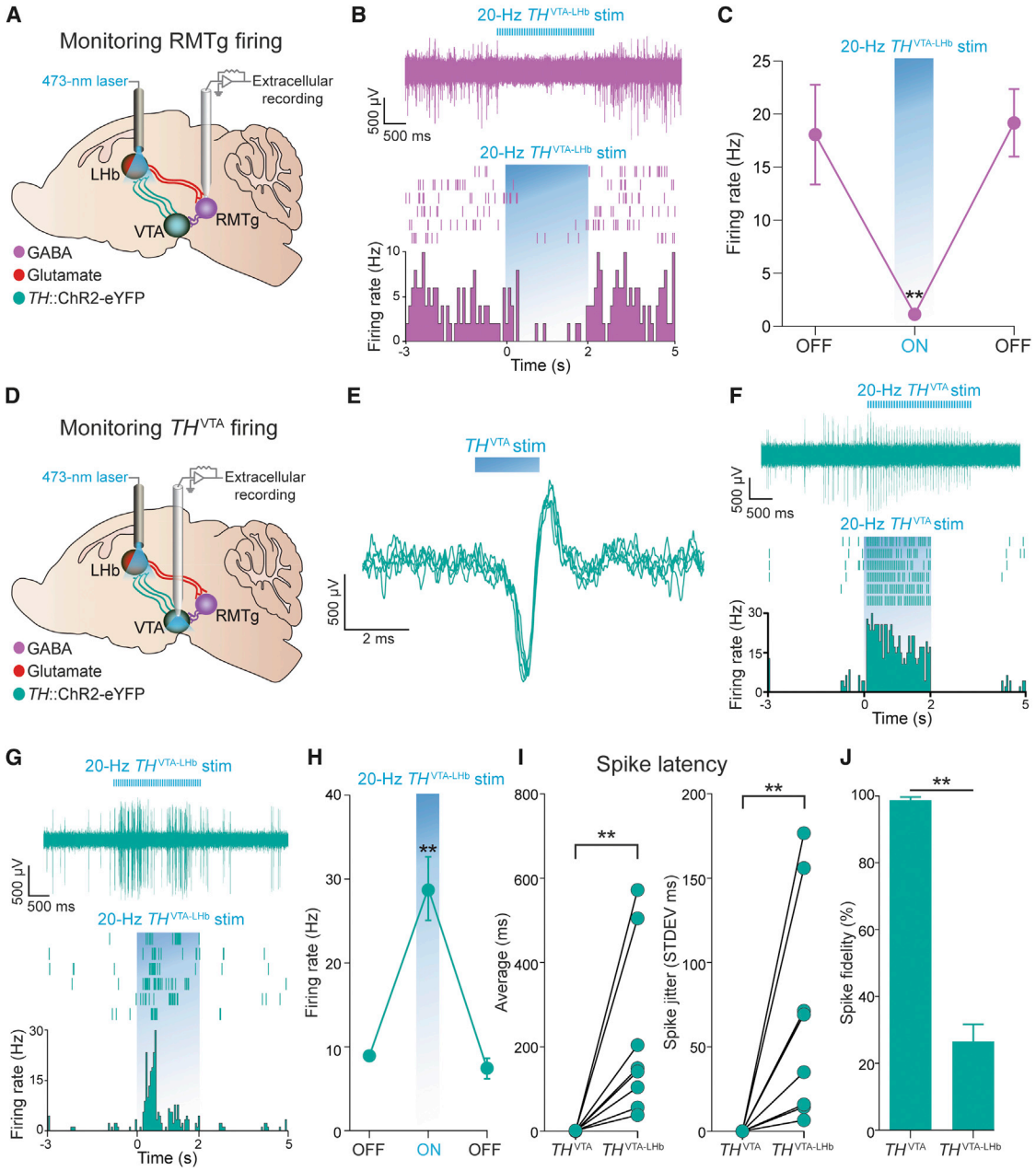

Figure 6. In Vivo Optical Stimulation of $TH^{VTA\text{-}LHb}$ Terminals Suppresses RMTg Activity and Enhances Spontaneous Firing of TH^{VTA} Neurons

(A) A schematic depicting anesthetized in vivo electrophysiological recordings from RMTg neurons during $TH^{VTA\text{-}LHb}$ terminal optical stimulation.

(B) Example trace from a single RMTg unit (top) and its representative peri-event histogram and raster (bottom) demonstrating repeated attenuation of firing to 20 Hz optical stimulation of the $TH^{VTA\text{-}LHb}$ pathway.

(C) Off, On, Off: before, during, after 20 Hz photostimulation (3 s each; 20 trials). The average firing rate of RMTg units significantly decreased during the 3 s 20 Hz optical stimulation trials ($F[2,15] = 4.33$, $p = 0.03$, $n = 3$ mice, $n = 6$ units). See also Figure S5.

(D) Schematic for anesthetized in vivo extracellular recordings in the VTA.

(E) Example traces from a single optically-tagged TH^{VTA} unit displaying repeated time-locked activation to 2 ms optical stimulation of the VTA.

(F) Example trace from a single TH^{VTA} unit (top) and its representative peri-event histogram and raster (bottom) displaying repeated time-locked activation to 20 Hz optical stimulation of TH^{VTA} cell bodies.

(G) Example trace from a single TH^{VTA} unit (top) and its representative peri-event histogram and raster (bottom) displaying enhanced activity in response to 20 Hz optical stimulation of $TH^{VTA\text{-}LHb}$ terminals within the LHb.

(H) The average firing rate of optically-identified TH^{VTA} units significantly increased during 20 Hz optical stimulation of $TH^{VTA\text{-}LHb}$ terminals within the LHb ($F[2,12] = 10.02$, $p = 0.0028$, $n = 3$ mice, $n = 5$ units).

(I) The average latency of each optical stimulation parameter (soma versus terminal; left) demonstrates that optical stimulation of $TH^{VTA\text{-}LHb}$ terminals resulted in significantly greater spike latencies in optically-identified TH^{VTA} neurons compared to light-evoked spikes from TH^{VTA}-soma optical stimulation ($p = 0.0053$,

(legend continued on next page)

the LHb increases dopamine release in the forebrain (Lecourtier et al., 2008). LHb neurons show a decrease in firing in response to cues that predict reward (Matsumoto and Hikosaka, 2007). Thus, we suggest that the phasic dopamine release seen in the NAc in response to motivationally relevant stimuli, at least in part, could require activation of inhibitory afferents to LHb, thus disinhibiting midbrain dopaminergic neurons. Data presented here demonstrate that a hybrid population of VTA neurons expressing dopaminergic and GABAergic markers send an inhibitory projection to the LHb and thus are able to directly inhibit LHb neurons, resulting in profound downstream effects on midbrain circuitry. This provides a circuit mechanism by which activation of the VTA-to-LHb pathway could promote reward.

Along with a robust excitatory projection to GABAergic neurons in the RMTg and posterior VTA, the LHb also sends a modest direct glutamatergic projection to VTA dopaminergic neurons (Balcita-Pedicino et al., 2011; Stamatakis and Stuber, 2012). If the VTA dopaminergic neurons that receive a direct connection from the LHb also project back to the LHb, this could provide an elegant negative feedback mechanism, whereby activation of the LHb would result in activation of $TH^{VTA\text{-}LHb}$ neurons, which in turn would shut down LHb activity.

Although the presence of a mesohabenular pathway has been recognized for many years (Phillipson and Griffith, 1980; Swanson, 1982), the present study characterizes the behavioral and functional relevance of this pathway. Our data add to the mounting evidence that dopaminergic neurons within the VTA are heterogeneous with respect to their electrophysiological and molecular profiles, their projection targets, and neurotransmitter signaling modalities. Further, our data demonstrate that the LHb and midbrain interact in a reciprocal manner and implicate the VTA's projection to the LHb as a key node in the classical midbrain reward circuit. This mechanistic framework underscores the flexibility and complexity of the circuitry that impinges upon VTA dopaminergic neurons to promote motivated behavior.

EXPERIMENTAL PROCEDURES

Subjects and Stereotactic Surgery

Adult (25–30 g) mice were group housed until surgery and maintained on a reverse 12 hr light cycle (lights off at 8:00) with ad libitum access to food and water. Mice were anesthetized with ketamine (150 mg/kg of body weight) and xylazine (50 mg/kg) and placed in a stereotactic frame (Kopf Instruments). For all slice electrophysiology and fast-scan cyclic voltammetry experiments, except for the retrobeads experiments, male and female *TH*-IRES-Cre backcrossed to C57BL/6J were bilaterally microinjected with 0.5 μl of purified and concentrated adeno-associated virus serotype 5 (AAV5; $\sim 10^{12}$ infections units per ml, packaged and titered by the UNC Vector Core Facility) into the VTA. Stereotactic coordinates are available in the Supplemental Experimental Procedures. Each VTA was injected with an AAV5 coding Cre-inducible ChR2 under control of the EF1α promoter to transduce VTA dopaminergic neurons (TH^{VTA}::ChR2). For the retrobead slice electrophysiology and PCR retrobead experiments, male and female *TH*-IRES-GFP mice received quadruple injections of 0.3 μl of red retrobeads (Lumafluor) into either the NAc or LHb. For the retrobead mapping and quantification experiments, male C57BL/6J mice (Jackson Laboratory) received quadruple injections with 0.3 μl of red retrobeads into the NAc. In the same surgery, the mice also received quadruple injections of 0.3 μl with green retrobeads (Lumafluor) into the LHb. For tracing experiments, *TH*-IRES-Cre mice were bilaterally injected with 0.5 μl of HSV-EF1α-LS1L-flp into the LHb or NAc and bilaterally injected with 0.5 μl of AAV5-EF1α-fdhChR2(H134R)-eYFP into the VTA. A detailed description of the HSV vector construction is available in the Supplemental Experimental Procedures. For behavioral experiments, male *TH*-IRES-Cre positive ($TH^{VTA\text{-}LHb}$::ChR2) and negative ($TH^{VTA\text{-}LHb}$::Control) littermates were bilaterally injected with Cre-inducible ChR2 and also implanted with bilateral chronic fibers directed above the LHb. For the LHb microinjection experiments, a 26G steel tube cannula (McMasters-Carr) that terminated 0.5 mm above the tip of the optical fiber was epoxied to an optical fiber and bilaterally aimed at the LHb. Retrobead experiments were performed 7–21 days after surgery. All other experiments were performed 6–8 weeks after surgery. Histology, immunohistochemistry, confocal, and electron microscopy procedures can be found in the Supplemental Experimental Procedures. All procedures were conducted in accordance with the Guide for the Care and Use of Laboratory Animals, as adopted by the US National Institutes of Health, and with approval of the UNC Institutional Animal Care and Use Committees.

Slice Preparation for Single-Cell RT-PCR, Fast-Scan Cyclic Voltammetry, and Patch-Clamp Electrophysiology

Mice were anesthetized with pentobarbital and perfused transcardially with modified artificial cerebrospinal fluid. Electrophysiological solutions can be found in the Supplemental Experimental Procedures. Brains were then rapidly removed and placed in the same solution that was used for perfusion at ~0°C. For the PCR experiments, horizontal slices containing the VTA (200 μm) were cut on a Vibratome (VT-1200, Leica Microsystems). For fast-scan cyclic voltammetry, coronal slices containing either the NAc (250 μm), (BNST 250 μm), or LHb (250 μm) were obtained. For patch-clamp electrophysiology, coronal slices containing the LHb (200 μm), or horizontal slices containing the VTA (200 μm) were obtained. Following slicing, brain slices were placed in a holding chamber and were allowed to recover for at least 30 min before being placed in the recording chamber and superfused with bicarbonate-buffered solution saturated with 95% O_2 and 5% CO_2.

RT-PCR

Electrophysiological solutions, equipment, and recording procedures can be found in the Supplemental Experimental Procedures. Autoclaved patch electrodes (2.0–2.5 MΩ) were backfilled with ~3–5 μl of a potassium chloride internal solution. Two microliters of RNase inhibitor (ANTI-RNase, Life Technologies) were added per 1 ml of the potassium chloride internal solution. Holding current was measured for no more than 3 min to minimize potential mRNA degradation. The cytoplasm was then aspirated by applying negative pressure and the integrity of the seal was monitored during aspiration to prevent extracellular contamination. Cells that showed more than a 100-pA change in holding current during aspiration were discarded. Immediately following aspiration, the pipette was removed from the tissue and the tip was broken into an RNase-free PCR tube. The solution inside the pipette was then injected into the RNase-free tube using positive pressure. Between each cell recording, the silver wire located inside the recording pipette was wiped thoroughly with 70% alcohol to minimize cross sample contamination. Finally, to control for pipette contamination, after each five consecutive

n = 3 mice, n = 9 units). The standard deviation (STDEV) of each stimulation type (right) shows that light-evoked spikes from TH^{VTA}-soma optical stimulation displayed significantly greater latency stability compared to $TH^{VTA\text{-}LHb}$-terminal initiated spikes ($p = 0.0014$, n = 3 mice, n = 9 units).
(J) TH^{VTA}-soma light-evoked spikes responded more reliably to 20 Hz optical stimulation compared to $TH^{VTA\text{-}LHb}$-terminal light-evoked spikes ($F[1,18] = 11.2$, $p = 0.0036$, n = 3 mice, n = 11 units). Error bars represent SEM. **$p < 0.01$ (Student's t test and ANOVA followed by Bonferroni post hoc comparisons, where applicable).

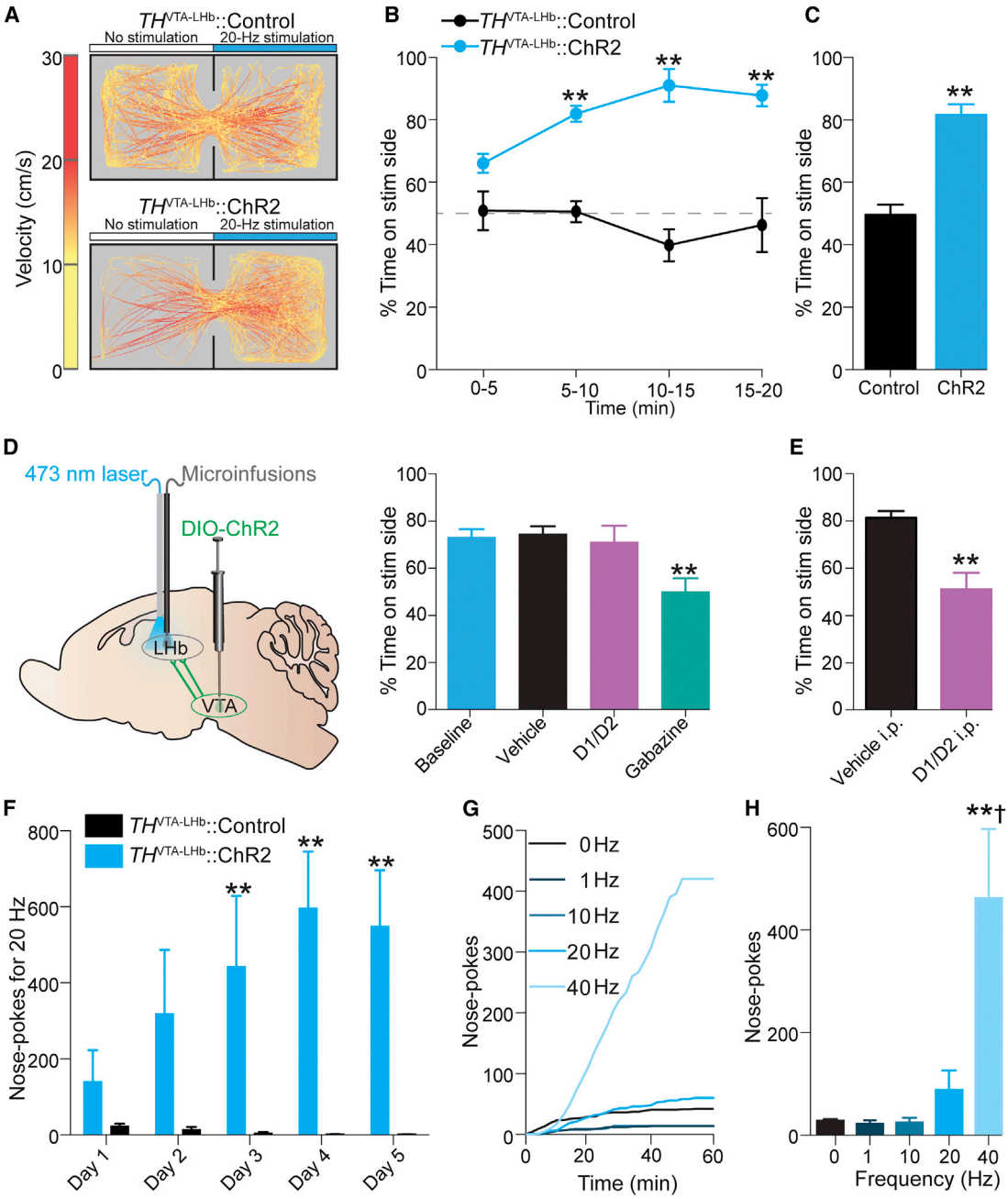

Figure 7. Activation of $TH^{VTA\text{-}LHb}$ Terminals Produces Reward-Related Behavioral Phenotypes

(A) Representative tracks from $TH^{VTA\text{-}LHb}$::Control (top) and $TH^{VTA\text{-}LHb}$::ChR2 (bottom) mice during RTPP task.

(B and C) $TH^{VTA\text{-}LHb}$::ChR2 mice spent more time on the side of the chamber paired with stimulation than $TH^{VTA\text{-}LHb}$::Control mice (5 min time bins: $F[3,1] = 79.2$, $p < 0.0001$; entire 20 min session: $t[13] = 8.82$, $p < 0.0001$; n = 8 $TH^{VTA\text{-}LHb}$::Control and 7 $TH^{VTA\text{-}LHb}$::ChR2). See also Figure S6.

(D) Intra-LHb injections of a $GABA_A$ antagonist, but not a dopamine receptor (D1 and D2) antagonist cocktail, followed by $TH^{VTA\text{-}LHb}$::ChR2 stimulation blocked the real-time place preference ($F[3,32] = 5.1$, $p = 0.005$; n = 9 mice).

(E) Systemic injection of a dopamine receptor (D1 and D2) antagonist cocktail followed by $TH^{VTA\text{-}LHb}$::ChR2 stimulation blocked the real-time place preference ($t[12] = 4.0$, $p = 0.002$; n = 7 mice).

(F) Active nose-poke responses from $TH^{VTA\text{-}LHb}$::ChR2 and $TH^{VTA\text{-}LHb}$::Control mice over the first 5 days of training. $TH^{VTA\text{-}LHb}$::ChR2 mice made significantly more nose-pokes on Days 3, 4, and 5 than $TH^{VTA\text{-}LHb}$::Control mice (Day 3: $t[12] = 3.78$, $p < 0.01$; Day 4: $t[12] = 4.45$, $p < 0.001$; Day 5: $t[12] = 4.22$, $p < 0.001$).

(G) Example cumulative records of nose-pokes made by a $TH^{VTA\text{-}LHb}$::ChR2 mouse for 0, 1, 10, 20, and 40 Hz optical stimulation in the 5-choice nose-poke task.

(H) $TH^{VTA\text{-}LHb}$::ChR2 mice made significantly more nose-pokes for 40 Hz than any other frequency ($F[4,25] = 9.13$, $p < 0.0001$). n = 6 $TH^{VTA\text{-}LHb}$::ChR2 mice. n = 8 $TH^{VTA\text{-}LHb}$::Control mice. Dagger symbol denotes significance compared to all manipulations. Error bars represent SEM. **$p < 0.01$ (Student's t test and ANOVA followed by Bonferroni post hoc comparisons, where applicable). See also Figure S7.

recordings, a recording pipette was lowered into the tissue with positive pressure, but without aspiration (tissue-stick control) and was then processed for quantitative PCR. Single-cell gene expression profiling and single-cell gene analysis are described in the Supplemental Experimental Procedures.

Fast-Scan Cyclic Voltammetry

Equipment, recording procedures, and analysis can be found in the Supplemental Experimental Procedures. T-650 carbon fiber microelectrodes (100–200 μm in length) were used for detection of dopamine in brain slices. Electrodes were placed in the NAc core, dorsal lateral BNST, or LHb of TH^{VTA}::ChR2 brain slices. Every 100 ms, the potential applied to the electrode was ramped from −0.4 V to +1.3 V to −0.4 V versus a Ag/AgCl reference wire at a rate of 400 V/s. To increase the sensitivity to detect dopamine with fast-scan cyclic voltammetry, slices were prepared as described above, but were incubated in aCSF containing 1 μM GBR12909 and 10 μM raclopride for at least 1 hr before recording. Prior to recording, slices were preperfused with L-Dopa (10 μM) for 10 min. Additionally, the electrode was ramped from −0.6 to 1.4 V to −0.6 V versus a Ag/AgCl reference wire at a rate of 400 V/s.

Patch-Clamp Electrophysiology

Electrophysiological solutions, equipment, recording procedures, and bath-applications of drugs can be found in the Supplemental Experimental Procedures. For the retrobeads experiments, whole-cell voltage clamp and cell-attached recordings were made from GFP+ neurons containing red retrobeads in the VTA. I_h current was measured by voltage-clamping the cell and stepping from −70 mV to −105 mV in 5 mV steps. For voltage-clamp recordings in LHb neurons, membrane potentials were maintained at −70 mV, and light pulses were delivered every 20 s to evoke neuronal firing. For cell-attached recordings, a 20-Hz optical stimulation was delivered for 1 s every 20 s for 20 sweeps. Firing rate was averaged across all 20 sweeps.

In Vivo Circuit Activity Mapping of the $TH^{VTA\text{-}LHb}$ Pathway

Surgical procedures, recordings, and analysis are described in the Supplemental Experimental Procedures. For monitoring RMTg and VTA neural firing during optical stimulation of the $TH^{VTA\text{-}LHb}$ pathway, the recording electrode was lowered separately into the RMTg (−3.9 mm posterior to bregma, ±0.9 mm lateral to midline, and –3.6 mm ventral to skull surface) and VTA (−3.1 mm posterior to bregma, ±0.4 mm lateral to midline, and −5.0 mm ventral to skull surface) by a motorized micromanipulator (Scientifica). To optically stimulate $TH^{VTA\text{-}LHb}$ terminals, an optical fiber coupled to a solid state laser (473 nm) was situated within a guide cannula and placed directly above the LHb at a 15° angle (−1.7 mm posterior to bregma, ±1.25 mm lateral to midline, and –3.24 mm ventral to skull surface). Train pulses of light (20 Hz) were delivered to the LHb every 3 s for 20 trials (each trial having 2 s prestimulation, 2 s stimulation, and 1 s poststimulation periods; Off, On, Off). To optically stimulate RMTg and VTA cell bodies, an optical fiber was fed through the side port of the electrode holder to terminate near the tip of the glass recording electrode. Recorded units were classified as light-responsive neurons if reliable light-evoked spikes were detected during the presentation of 2-ms light pulses (20 trials each).

In Vivo Optogenetic Experiments

Real-time place preference procedures, optical self-stimulation, and 5-choice self-stimulation procedures were conducted as previously described (Jennings et al., 2013; Stamatakis and Stuber, 2012; see Supplemental Experimental Procedures).

SUPPLEMENTAL INFORMATION

Supplemental Information includes Supplemental Experimental Procedures and seven figures and can be found with this article online at http://dx.doi.org/10.1016/j.neuron.2013.08.023.

ACKNOWLEDGMENTS

We thank V. Gukassyan and the University of North Carolina (UNC) Neuroscience Center Microscopy Core (P30 NS045892), and the members of the Stuber laboratory for discussion. We thank Kristen Phend and Susan Burette for technical assistance with histology and electron microscopy. We thank the UNC Vector Core Facility for viral packaging. This study was supported by The Whitehall Foundation, the Brain and Behavior Research Foundation (NARSAD), The Foundation of Hope, and National Institutes of Health grants DA032750 (to G.D.S), DA034472 (to A.M.S), and NS039444 (to R.J.W.)

Accepted: August 21, 2013
Published: November 20, 2013

REFERENCES

Adell, A., and Artigas, F. (2004). The somatodendritic release of dopamine in the ventral tegmental area and its regulation by afferent transmitter systems. Neurosci. Biobehav. Rev. *28*, 415–431.

Balcita-Pedicino, J.J., Omelchenko, N., Bell, R., and Sesack, S.R. (2011). The inhibitory influence of the lateral habenula on midbrain dopamine cells: ultrastructural evidence for indirect mediation via the rostromedial mesopontine tegmental nucleus. J. Comp. Neurol. *519*, 1143–1164.

Barrot, M., Sesack, S.R., Georges, F., Pistis, M., Hong, S., and Jhou, T.C. (2012). Braking dopamine systems: a new GABA master structure for mesolimbic and nigrostriatal functions. J. Neurosci. *32*, 14094–14101.

Bass, C.E., Grinevich, V.P., Kulikova, A.D., Bonin, K.D., and Budygin, E.A. (2013). Terminal effects of optogenetic stimulation on dopamine dynamics in rat striatum. J. Neurosci. Methods *214*, 149–155.

Beckstead, M.J., Grandy, D.K., Wickman, K., and Williams, J.T. (2004). Vesicular dopamine release elicits an inhibitory postsynaptic current in midbrain dopamine neurons. Neuron *42*, 939–946.

Brinschwitz, K., Dittgen, A., Madai, V.I., Lommel, R., Geisler, S., and Veh, R.W. (2010). Glutamatergic axons from the lateral habenula mainly terminate on GABAergic neurons of the ventral midbrain. Neuroscience *168*, 463–476.

Bromberg-Martin, E.S., Matsumoto, M., and Hikosaka, O. (2010). Distinct tonic and phasic anticipatory activity in lateral habenula and dopamine neurons. Neuron *67*, 144–155.

Chaudhury, D., Walsh, J.J., Friedman, A.K., Juarez, B., Ku, S.M., Koo, J.W., Ferguson, D., Tsai, H.-C., Pomeranz, L., Christoffel, D.J., et al. (2013). Rapid regulation of depression-related behaviours by control of midbrain dopamine neurons. Nature *493*, 532–536.

Christoph, G.R., Leonzio, R.J., and Wilcox, K.S. (1986). Stimulation of the lateral habenula inhibits dopamine-containing neurons in the substantia nigra and ventral tegmental area of the rat. J. Neurosci. *6*, 613–619.

Cohen, J.Y., Haesler, S., Vong, L., Lowell, B.B., and Uchida, N. (2012). Neuron-type-specific signals for reward and punishment in the ventral tegmental area. Nature *482*, 85–88.

Cruikshank, S.J., Urabe, H., Nurmikko, A.V., and Connors, B.W. (2010). Pathway-specific feedforward circuits between thalamus and neocortex revealed by selective optical stimulation of axons. Neuron *65*, 230–245.

Day, J.J., Roitman, M.F., Wightman, R.M., and Carelli, R.M. (2007). Associative learning mediates dynamic shifts in dopamine signaling in the nucleus accumbens. Nat. Neurosci. *10*, 1020–1028.

Ford, C.P., Mark, G.P., and Williams, J.T. (2006). Properties and opioid inhibition of mesolimbic dopamine neurons vary according to target location. J. Neurosci. *26*, 2788–2797.

Grace, A.A. (1991). Phasic versus tonic dopamine release and the modulation of dopamine system responsivity: a hypothesis for the etiology of schizophrenia. Neuroscience *41*, 1–24.

Gruber, C., Kahl, A., Lebenheim, L., Kowski, A., Dittgen, A., and Veh, R.W. (2007). Dopaminergic projections from the VTA substantially contribute to the mesohabenular pathway in the rat. Neurosci. Lett. *427*, 165–170.

Hnasko, T.S., Hjelmstad, G.O., Fields, H.L., and Edwards, R.H. (2012). Ventral tegmental area glutamate neurons: electrophysiological properties and projections. J. Neurosci. *32*, 15076–15085.

Jennings, J.H., Sparta, D.R., Stamatakis, A.M., Ung, R.L., Pleil, K.E., Kash, T.L., and Stuber, G.D. (2013). Distinct extended amygdala circuits for divergent motivational states. Nature *496*, 224–228.

Jhou, T.C., Geisler, S., Marinelli, M., Degarmo, B.A., and Zahm, D.S. (2009). The mesopontine rostromedial tegmental nucleus: A structure targeted by the lateral habenula that projects to the ventral tegmental area of Tsai and substantia nigra compacta. J. Comp. Neurol. *513*, 566–596.

Jhou, T.C., Good, C.H., Rowley, C.S., Xu, S.-P., Wang, H., Burnham, N.W., Hoffman, A.F., Lupica, C.R., and Ikemoto, S. (2013). Cocaine drives aversive conditioning via delayed activation of dopamine-responsive habenular and midbrain pathways. J. Neurosci. *33*, 7501–7512.

Ji, H., and Shepard, P.D. (2007). Lateral habenula stimulation inhibits rat midbrain dopamine neurons through a GABA(A) receptor-mediated mechanism. J. Neurosci. *27*, 6923–6930.

Kim, U., and Lee, T. (2012). Topography of descending projections from anterior insular and medial prefrontal regions to the lateral habenula of the epithalamus in the rat. Eur. J. Neurosci. *35*, 1253–1269.

Knable, M.B., and Weinberger, D.R. (1997). Dopamine, the prefrontal cortex and schizophrenia. J. Psychopharmacol. (Oxford) *11*, 123–131.

Kowski, A.B., Veh, R.W., and Weiss, T. (2009). Dopaminergic activation excites rat lateral habenular neurons in vivo. Neuroscience *161*, 1154–1165.

Kuhlman, S.J., and Huang, Z.J. (2008). High-resolution labeling and functional manipulation of specific neuron types in mouse brain by Cre-activated viral gene expression. PLoS ONE *3*, e2005.

Lammel, S., Hetzel, A., Häckel, O., Jones, I., Liss, B., and Roeper, J. (2008). Unique properties of mesoprefrontal neurons within a dual mesocorticolimbic dopamine system. Neuron *57*, 760–773.

Lammel, S., Ion, D.I., Roeper, J., and Malenka, R.C. (2011). Projection-specific modulation of dopamine neuron synapses by aversive and rewarding stimuli. Neuron *70*, 855–862.

Lammel, S., Lim, B.K., Ran, C., Huang, K.W., Betley, M.J., Tye, K.M., Deisseroth, K., and Malenka, R.C. (2012). Input-specific control of reward and aversion in the ventral tegmental area. Nature *491*, 212–217.

Lecourtier, L., Defrancesco, A., and Moghaddam, B. (2008). Differential tonic influence of lateral habenula on prefrontal cortex and nucleus accumbens dopamine release. Eur. J. Neurosci. *27*, 1755–1762.

Lüscher, C., and Malenka, R.C. (2011). Drug-evoked synaptic plasticity in addiction: from molecular changes to circuit remodeling. Neuron *69*, 650–663.

Margolis, E.B., Lock, H., Hjelmstad, G.O., and Fields, H.L. (2006). The ventral tegmental area revisited: is there an electrophysiological marker for dopaminergic neurons? J. Physiol. *577*, 907–924.

Matsui, A., and Williams, J.T. (2011). Opioid-sensitive GABA inputs from rostromedial tegmental nucleus synapse onto midbrain dopamine neurons. J. Neurosci. *31*, 17729–17735.

Matsumoto, M., and Hikosaka, O. (2007). Lateral habenula as a source of negative reward signals in dopamine neurons. Nature *447*, 1111–1115.

McCulloch, J., Savaki, H.E., and Sokoloff, L. (1980). Influence of dopaminergic systems on the lateral habenular nucleus of the rat. Brain Res. *194*, 117–124.

Meier, C.L., and Herrling, P.L. (1993). N-methyl-D-aspartate induces regular firing patterns in the cat lateral habenula in vivo. Neuroscience *52*, 951–959.

Mercuri, N.B., Bonci, A., Calabresi, P., Stefani, A., and Bernardi, G. (1995). Properties of the hyperpolarization-activated cation current Ih in rat midbrain dopaminergic neurons. Eur. J. Neurosci. *7*, 462–469.

Newman-Tancredi, A., Cussac, D., Quentric, Y., Touzard, M., Verrièle, L., Carpentier, N., and Millan, M.J. (2002). Differential actions of antiparkinson agents at multiple classes of monoaminergic receptor. III. Agonist and antagonist properties at serotonin, 5-HT(1) and 5-HT(2), receptor subtypes. J. Pharmacol. Exp. Ther. *303*, 815–822.

Nirenberg, M.J., Chan, J., Liu, Y., Edwards, R.H., and Pickel, V.M. (1996). Ultrastructural localization of the vesicular monoamine transporter-2 in midbrain dopaminergic neurons: potential sites for somatodendritic storage and release of dopamine. J. Neurosci. *16*, 4135–4145.

Oleson, E.B., Gentry, R.N., Chioma, V.C., and Cheer, J.F. (2012). Subsecond dopamine release in the nucleus accumbens predicts conditioned punishment and its successful avoidance. J. Neurosci. *32*, 14804–14808.

Pan, W.-X., Schmidt, R., Wickens, J.R., and Hyland, B.I. (2005). Dopamine cells respond to predicted events during classical conditioning: evidence for eligibility traces in the reward-learning network. J. Neurosci. *25*, 6235–6242.

Phillips, P.E.M., Stuber, G.D., Heien, M.L.A.V., Wightman, R.M., and Carelli, R.M. (2003). Subsecond dopamine release promotes cocaine seeking. Nature *422*, 614–618.

Phillipson, O.T., and Griffith, A.C. (1980). The neurones of origin for the mesohabenular dopamine pathway. Brain Res. *197*, 213–218.

Poller, W.C., Madai, V.I., Bernard, R., Laube, G., and Veh, R.W. (2013). A glutamatergic projection from the lateral hypothalamus targets VTA-projecting neurons in the lateral habenula of the rat. Brain Res. *1507*, 45–60.

Schultz, W., Dayan, P., and Montague, P.R. (1997). A neural substrate of prediction and reward. Science *275*, 1593–1599.

Shabel, S.J., Proulx, C.D., Trias, A., Murphy, R.T., and Malinow, R. (2012). Input to the lateral habenula from the basal ganglia is excitatory, aversive, and suppressed by serotonin. Neuron *74*, 475–481.

Shen, X., Ruan, X., and Zhao, H. (2012). Stimulation of midbrain dopaminergic structures modifies firing rates of rat lateral habenula neurons. PLoS ONE *7*, e34323.

Skagerberg, G., Lindvall, O., and Björklund, A. (1984). Origin, course and termination of the mesohabenular dopamine pathway in the rat. Brain Res. *307*, 99–108.

Sparta, D.R., Stamatakis, A.M., Phillips, J.L., Hovelsø, N., van Zessen, R., and Stuber, G.D. (2012). Construction of implantable optical fibers for long-term optogenetic manipulation of neural circuits. Nat. Protoc. *7*, 12–23.

Stamatakis, A.M., and Stuber, G.D. (2012). Activation of lateral habenula inputs to the ventral midbrain promotes behavioral avoidance. Nat. Neurosci. *15*, 1105–1107.

Stuber, G.D., Klanker, M., de Ridder, B., Bowers, M.S., Joosten, R.N., Feenstra, M.G., and Bonci, A. (2008). Reward-predictive cues enhance excitatory synaptic strength onto midbrain dopamine neurons. Science *321*, 1690–1692.

Stuber, G.D., Hnasko, T.S., Britt, J.P., Edwards, R.H., and Bonci, A. (2010). Dopaminergic terminals in the nucleus accumbens but not the dorsal striatum corelease glutamate. J. Neurosci. *30*, 8229–8233.

Swanson, L.W. (1982). The projections of the ventral tegmental area and adjacent regions: a combined fluorescent retrograde tracer and immunofluorescence study in the rat. Brain Res. Bull. *9*, 321–353.

Tecuapetla, F., Patel, J.C., Xenias, H., English, D., Tadros, I., Shah, F., Berlin, J., Deisseroth, K., Rice, M.E., Tepper, J.M., and Koos, T. (2010). Glutamatergic signaling by mesolimbic dopamine neurons in the nucleus accumbens. J. Neurosci. *30*, 7105–7110.

Tobler, P.N., Fiorillo, C.D., and Schultz, W. (2005). Adaptive coding of reward value by dopamine neurons. Science *307*, 1642–1645.

Tritsch, N.X., Ding, J.B., and Sabatini, B.L. (2012). Dopaminergic neurons inhibit striatal output through non-canonical release of GABA. Nature *490*, 262–266.

Tsai, H.-C., Zhang, F., Adamantidis, A., Stuber, G.D., Bonci, A., de Lecea, L., and Deisseroth, K. (2009). Phasic firing in dopaminergic neurons is sufficient for behavioral conditioning. Science *324*, 1080–1084.

Tye, K.M., Mirzabekov, J.J., Warden, M.R., Ferenczi, E.A., Tsai, H.-C., Finkelstein, J., Kim, S.-Y., Adhikari, A., Thompson, K.R., Andalman, A.S.,

et al. (2013). Dopamine neurons modulate neural encoding and expression of depression-related behaviour. Nature *493*, 537–541.

Ungless, M.A., Magill, P.J., and Bolam, J.P. (2004). Uniform inhibition of dopamine neurons in the ventral tegmental area by aversive stimuli. Science *303*, 2040–2042.

Warden, M.R., Selimbeyoglu, A., Mirzabekov, J.J., Lo, M., Thompson, K.R., Kim, S.-Y., Adhikari, A., Tye, K.M., Frank, L.M., and Deisseroth, K. (2012). A prefrontal cortex-brainstem neuronal projection that controls response to behavioural challenge. Nature *492*, 428–432.

Witten, I.B., Steinberg, E.E., Lee, S.Y., Davidson, T.J., Zalocusky, K.A., Brodsky, M., Yizhar, O., Cho, S.L., Gong, S., Ramakrishnan, C., et al. (2011). Recombinase-driver rat lines: tools, techniques, and optogenetic application to dopamine-mediated reinforcement. Neuron *72*, 721–733.